Journal of The Electrochemical Society

The Electrochemical Society
Advancing solid state & electrochemical science & technology

OPEN ACCESS

Studies of the Electrochemical Behavior of $LiNi_{0.80}Co_{0.15}Al_{0.05}O_2$ Electrodes Coated with $LiAlO_2$

To cite this article: Onit Srur-Lavi *et al* 2017 *J. Electrochem. Soc.* **164** A3266

Studies of the Electrochemical Behavior of $LiNi_{0.80}Co_{0.15}Al_{0.05}O_2$ Electrodes Coated with $LiAlO_2$

Onit Srur-Lavi,[a] Ville Miikkulainen,[b] Boris Markovsky,[a,*,z] Judith Grinblat,[a] Michael Talianker,[c] Yafit Fleger,[d] Gili Cohen-Taguri,[d] Albert Mor,[a] Yosef Tal-Yosef,[d] and Doron Aurbach[a,]**

[a]*Department of Chemistry Bar-Ilan University, Ramat-Gan 52900, Israel*
[b]*Department of Chemistry, University of Helsinki A. I. Virtasen aukio 1, 00560 Helsinki, Finland*
[c]*Department of Materials Engineering, Ben-Gurion University of the Negev, Beer-Sheva 84105, Israel*
[d]*Bar-Ilan Institute for Nanotechnology and Advanced Materials, Ramat-Gan 52900, Israel*

In this paper, we studied the influence of $LiAlO_2$ coatings of 0.5, 1 and 2 nm thickness prepared by Atomic Layer Deposition onto $LiNi_{0.8}Co_{0.15}Al_{0.05}O_2$ electrodes, on their electrochemical behavior at 30 and 60°C. It was demonstrated that upon cycling, 2 nm $LiAlO_2$ coated electrodes displayed ~3 times lower capacity fading and lower voltage hysteresis comparing to bare electrodes. We established a correlation among the thickness of the $LiAlO_2$ coating and parameters of the self-discharge processes at 30 and 60°C. Significant results on the elevated temperature cycling and aging of bare and $LiAlO_2$ coated electrodes at 4.3 V were obtained and analyzed for the first time. By analyzing of X-ray diffraction patterns of bare and 2 nm coated $LiNi_{0.8}Co_{0.15}Al_{0.05}O_2$ electrodes after cycling, we concluded that cycled materials preserved their original structure described by *R-3m* space group and no additional phases were detected.

Manuscript submitted September 5, 2017; revised manuscript received October 17, 2017. Published October 28, 2017.

The lithium-ion batteries (LIB) market nowadays has expanded widely from cellular phones, computers and other electronic devices to the automotive industry. Positive electrodes for LIBs to be explored in electric vehicles are mainly based on lithiated transition-metal oxides comprising Ni, Co and Mn ($LiNi_yCo_xMn_{1-y-x}O_2$) and designated as NCM.[1,2] They have attracted much attention as promising materials and therefore many research projects have been dedicated to them in the past 20 years.[3–13] In studies of $LiNi_{1/3}Co_{1/3}Mn_{1/3}O_2$ (NCM333) cathodes, it was demonstrated[4–6] that they provided a capacity of 200 mAh/g in the voltage range of 2.5–4.6 V, or ~155 mAh/g if the cutoff voltage is limited by 4.3 V.[7] A substantially improved high-voltage performance of NCM333 electrodes (up to 4.6 V) was achieved by introducing tris(2,2,2-trifluoroethyl) borate additive in the electrolyte solution.[8] These authors suggest that the additive takes part in the formation of the solid-electrolyte interface by lowering and stabilization of the interfacial resistance. NCM333 and NCM424 materials were studied in our group from the viewpoint of their electrochemical behavior, aging mechanisms, thermal properties, and surface chemistry developed upon cycling in ethylene carbonate-dimethyl carbonate/$LiPF_6$ based solutions.[9] $LiNi_yCo_xMn_{1-y-x}O_2$ materials with higher Ni content ($y > 5$) are important due to high capacity that can be extracted by charging up to 4.3 V only. However, Ni-rich NCMs suffer from their low cycling stability especially for compositions with Ni ≥ 60%, severe capacity fading and impedance increase during cycling at elevated temperatures (e.g. 45°C). One of the effective ways to stabilize the structure of NCM materials, to increase cycling activity and to diminish the heat evolution of the electrodes in a charged state is lattice doping with various cations like Al^{3+}, Ti^{4+}, Zr^{4+}, Zn^{2+}, Fe^{3+}, Cu^{2+}, and Cr^{3+}.[10] It was demonstrated, for instance, that the lower capacity fading of the Al-doped $LiNi_{0.5}Co_{0.2}Mn_{0.3}O_2$ (NCM523) electrodes upon cycling and aging of the cells in a charged state (4.3 V) at 60°C are likely due to the chemical and structural modifications of the electrode/solution interface.[10] Recently, Li et al. have shown that co-modification of NCM523 by bulk doping with zirconium and surface coating with polypyrrole conductive film resulted in substantially enhanced capacity retention of these electrodes cycled to 4.6 V.[11] In a systematic study[12] of the Al-doped Ni-rich electrodes $LiNi_{0.8}Co_{0.15}Al_{0.05}O_2$ which are promising materials for use in batteries for electromotive applications the authors have shown high cycling stability upon accelerated testing. $LiNi_{0.8}Co_{0.15}Al_{0.05}O_2$ electrodes demonstrate reversible capacities of ~200 mAh/g in the range of 3.0–4.2 V; the material has lower cost and is more environmentally friendly comparing to other compositions.[1,2,13] However, NCA electrodes show structural instability, poor cycling behavior at high rates, elevated temperatures and in wide potential ranges, as well as capacity losses of up to 30%.[14] There is a consensus in the literature that the above drawbacks originate from the unstable Ni^{4+} ions developed in the charge state (high anodic potential, most Li^+ extracted from NCA). These Ni-ions can be readily reduced to more favorable valence states accompanied by phase transitions, as described, for instance in Ref. 15. The discharge capacity of NCA electrodes can be increased by about 10% if operating to higher upper cutoff potentials (vs. Li metal), increasing thus the overall energy density of the material. On the other hand, charging above 4.2 V leads to a faster structural instability caused by the oxygen loss, generation of microstrains, and to degradation of the material.[16,17] Degradation also occurs during storage at elevated temperatures (60°C) due to accelerated interfacial reactions with battery solutions.[17] One of the promising approaches to eliminate the above mentioned drawbacks of NCA and NCM materials is their coating (surface modification) with thin surface layers, like SiO_2 and $Ni_3(PO_4)_2$.[18–20] The main objective is to protect the surface area of the cathode material by an inert thin layer of organic or inorganic compounds. The coating acts as a barrier between the active material and the electrolyte minimizing parasitic side reactions at high voltages by partial reactions with HF (scavenging) that is especially beneficial if the coating is not uniform or tends to break during cycling.[21] Numerous coatings have been investigated up till now for different NCMs, for instance AlF_3,[22] Al_2O_3,[23] TiO_2,[24] SiO_2[25] demonstrating improved cycling stability of the electrodes when coatings used in low amounts. In order to minimize the ion resistance, lithium containing thin films of Li_3N, LiF, $LiAlO_2$, LiPON, $LiFePO_4$ and $LiAlF_4$ were shown to improve cycling performance and voltage windows of Ni-rich NCM materials.[26] The coatings do not contribute to the electrode capacity and hence high amounts will lower the specific capacity of the active material.[23] Since side reactions are minimal in coated samples, a lower impedance growth is usually observed during cycling.[24] One of the efficient processes for coating is atomic layer deposition (ALD) that was shown to be an alternative technique with several important advantages over the others.[27–29] For instance, the coating thickness can be tailored just by the number of ALD cycles and furthermore the coating is uniform amongst all secondary particles. Consequently, improvements in the capacity retention, the rate capability and the

*Electrochemical Society Member.
**Electrochemical Society Fellow.
[z]E-mail: markovskyboris22@gmail.com

electrochemical behavior at high temperature can be achieved.[26,30–34] The use of ALD coating enables a super conformal coating and creates an artificial Solid Electrolyte Interphase (SEI) that serves as a passivating layer on the electrodes.[35–37] Recently, ALD amorphous coatings by TiO_2 and Al_2O_3 were used on NCA and Ni-rich NCM powders in order to improve the cycling behavior and structural stability of cathodes at 25 and 55°C.[38,39] It should be noted however that the information in the literature about coatings (for instance, of $LiAlO_2$ films) prepared by ALD on NCM or NCA electrodes (not on active powders) is limited.[37] Moreover the electrochemical behavior of bare and coated NCA samples as cathodes in Li-cells at elevated temperatures has not been fully studied yet.[40,41]

Therefore, one of the motivating factors of the present work was to understand the influence of nano-sized $LiAlO_2$ coatings prepared by ALD onto $LiNi_{0.8}Co_{0.15}Al_{0.05}O_2$ electrodes on their electrochemical behavior at 30 and 60°C in terms of the potential windows, capacity fade, impedance characteristics, and the self-discharge. Hence, with this in mind, $LiAlO_2$ coatings of 0.5, 1 and 2 nm thickness were effectively deposited directly onto $LiNi_{0.8}Co_{0.15}Al_{0.05}O_2$ electrodes using ALD technique. We characterized the coatings of ∼30 nm thick on nickel foil ("model electrode") by HRTEM imaging, nano-beam electron diffraction, and grazing-incidence XRD measurements. Electrochemical studies of NCA bare and $LiAlO_2$ coated electrodes included cycling behavior up to 4.4–4.5 V, impedance during the Li^+ deintercalation, and the self-discharge in Li-cells at 30 and 60°C. An important goal of this study was also to attest possible structural changes of bare and coated electrodes due to cycling. The novelty of the present research is that, for the first time, we obtained and analyzed significant results on the elevated temperature aging (the self-discharge) of bare and $LiAlO_2$ coated electrodes at 4.3 V. This paper continues our recent works on NCM and NCA electrodes in Li-cells.[10,42–44]

Experimental

Materials, electrodes, and electrochemical cells assembling.— $LiNi_{0.8}Co_{0.15}Al_{0.05}O_2$ material for positive electrodes (cathodes) of lithium cells was received from Toda (Japan). Working electrodes for electrochemical cells were prepared by mixing the active material NCA with carbon black super P (from Timcal), graphite KS-6 (Timcal) and binder PVdF (Kynar HSV900) in a ratio of 88:4:4:4 wt%, in N-methyl pirollidone using Thinky Planetary Vacuum Mixer (Japan) to obtain slurry. It was then cast onto an aluminum foil (15 μm thick, from Strem) and dried on a hotplate followed by drying at 120°C under vacuum overnight. The average loading of the active mass was ∼5 mg/cm^2. These electrodes were coated by $LiAlO_2$ (LAO) layers of 0.5, 1 and 2 nm thick (using 3, 6, and 12 ALD cycles, respectively) by Atomic Layer Deposition (ALD) method, at the Department of Chemistry, University of Helsinki, Finland. They are nominated as NCA/LAO-05, NCA/LAO-1 and NCA/LAO-2, respectively throughout the paper. LAO films were deposited with Picosun R-150 ALD reactor from trimethylaluminum (TMA, Chemtura Manufacturing UK), lithium tert-butoxide (99% LiO^{t}Bu, Alfa Aesar) and deionized water at a deposition temperature of 225°C. TMA and water were held at room temperature and pulsed from external vessels whereas LiO^{t}Bu was evaporated from a heated source held at 160°C. Reactor pressure was in the order of 5 mbar, maintained by mass flow controlled, constant nitrogen (99.999% N_2) flow and vacuum pump. The deposition process variables and the film uniformity were first optimized on 150-mm silicon wafers. The optimal ALD cycle was 0.1 s TMA pulse-5 s purge-0.1 s water pulse-5 s purge-0.5 s LiOtBu pulse-5 s purge-0.1 s water pulse-5 s purge resulting in 1.6 Å $LiAlO_2$ growth per cycle uniformly over the silicon wafer, corresponding well to the value reported in the literature.[45] The thicknesses of 20–100 nm $LiAlO_2$ films were measured on Si wafers with X-ray reflection. These measurements gave 1.6 Å $LiAlO_2$ growth per cycle that was extrapolated to targeted thicknesses of 0.5, 1 and 2 nm, as the direct thickness analysis of such thin films on heterogeneous electrode sheets is very challenging. Electrode strips after ALD coating were kept under Nitrogen/Argon atmosphere. Electrodes for electrochemical testing were punched as discs (14 mm in diameter) from the electrode strips (bare and LAO coated) and used for fabrication of two- and three-electrode 2325 coin-type cells, as described in previous papers.[46,47] Lithium foil (200 μm thick) and Celgard PP2500 polypropylene membrane served as anode and separator, respectively. We also prepared pouch cells comprising NCA-bare or NCA/LAO electrodes of the geometric surface area ∼35 × 30 mm (loading ∼5 mg/cm^2) and lithium foil and Li-chip as counter and reference electrodes. Electrochemical cells were assembled in glove boxes (VAC, Inc.) filled with highly pure argon 99.999%. For electrochemical measurements, we used electrolyte solutions (Li battery grade) of ethylmethyl carbonate (EMC) and ethylene carbonate (EC) (weight ratio of 7:3) with 1 M $LiPF_6$ (from BASF). The cells were kept under OCV for 12 h prior to testing to ensure full wetting of electrodes and separators with electrolyte solutions. The electrochemical tests were performed using multi-channel battery testers from Maccor Inc. (USA) and BTU-1470 (Solartron) equipped with frequency response analyzer FRA-1255 (driven by Corrware and ZPlot software, Scribner Associates, Inc.) The alternating voltage amplitude in impedance measurements was 3 mV and the frequency ranged from 100 kHz to 5 mHz. All the potentials in this paper are given vs. Li/Li^+. Three identical cells were tested simultaneously for statistical purposes; the accuracy of the calculations of electrodes' capacity was ∼95%. For the self-discharge tests, the electrochemical cells comprising bare or coated NCA cathodes were galvanostatically cycled at a C/5 rate at 30°C, terminated at 4.3 V, kept at this potential for 5 hours and subsequently aged either at 30°C or at 60°C (in thermostats) for 1 week. After these experiments, the cells were cycled at a C/5 rate at 30°C, starting from the discharge step.

X-ray diffraction (XRD) and transmission electron microscopy (TEM).— X-ray diffraction measurements of the bare and NCA/LAO-05, NCA/LAO-1 and NCA/LAO-2 electrodes (before and after electrochemical cycling) were performed using an AXS D8 Advance diffractometer from Bruker, Inc. (Germany) in the 2θ range from 10° to 110°, with a step size of 0.02°, at 15 sec/step rate. To examine the structure of the $LiAlO_2$ coating by TEM and by XRD grazing-incidence technique (GIXRD) $LiAlO_2$ film, ∼30 nm thick, was specially deposited by ALD only on the clean Ni foil. GIXRD measurements of the $LiAlO_2$ film prepared onto Ni-foil by ALD were carried out using a Rigaku Smartlab X-ray diffractometer, employing parallel beam optics, the latter with a fixed low incident angle of 1.5°. Data were collected in 2θ range from 10° to 80°, with a scanning rate of 0.1°/min. The X-ray generator was operated at 40 kV and 30 mA with Cu-Kα radiation (λ = 1.5419 Å). TEM examinations of the $LiAlO_2$ film deposited onto nickel foil was performed with a JEOL JEM-2100 (LaB6) high resolution electron microscope. Selected area electron diffraction (SAED) and convergent beam electron diffraction (CBED) techniques (4–7 nm probe size) were employed for structural characterization of nanoparticles. Samples for these studies were prepared from scratched $LiAlO_2$ particles using methodology described in Ref. 48 as well as by Focusing Ion Beam (FIB) method using cross-sections produced with a Helios 600 dual beam instrument and transferred to the transmission electron microscope in vials filled with Argon.

Results and Discussion

Structural studies of $LiAlO_2$ layers prepared by ALD on the Nickel substrates.— The microstructure of the $LiAlO_2$ layer (∼30 nm thick) deposited by ALD onto the nickel foil, as a "model electrode", can be seen in Figure 1a, which represents a STEM image of the FIB-prepared cross-section of the nickel foil/$LiAlO_2$ interface. The corresponding EDS line-scan profile (Figure 1b) clearly shows three regions, as follows: (1) the region of the Ni substrate, (2) the ALD-deposited layer of ∼ 30 nm thick; note, that the EDS detector only shows the presence of Al, (3) the Pt-layer, which is formed in the

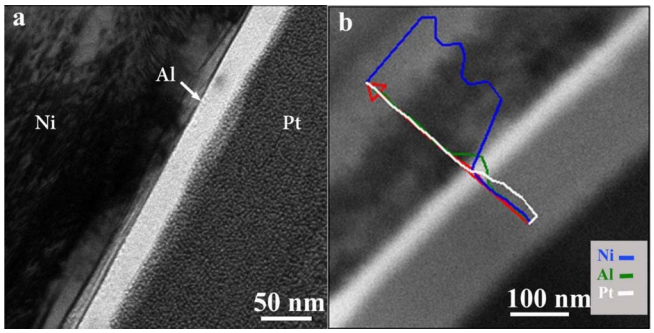

Figure 1. (a) STEM Bright Field image of the cross-section of the $LiAlO_2$ film prepared by ALD on the Ni-foil substrate (a "model electrode"). The thickness of the deposited layer is ~ 30 nm. The Pt layer seen in the image originates from the cross-sectioning process by FIB where Pt is being used. (b) Elemental line scans are shown for: Ni - blue, Al - green and Pt - white.

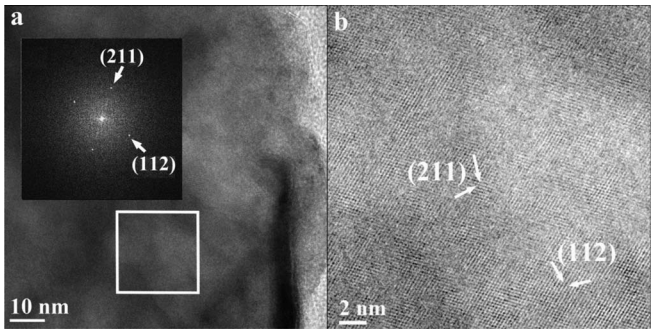

Figure 3. a) High Resolution TEM micrograph of the crystalline area of the $LiAlO_2$ layer deposited on Ni-foil by ALD. The insert shows fast Fourier transform (FFT) taken from the area marked by a white square. The "reflections" in FFT demonstrate the crystalline character of the region. (b) The processed image from the square area in (a) demonstrates clear lattice fringes of the (211) and (112) planes in the orthorhombic β-$LiAlO_2$ as seen in diffractions in Figure 2.

course of FIB preparation of the specimen. Although the particles deposited onto TEM-grid were heavily agglomerated (as can be seen in Figure 2a), nevertheless, it was possible to find some transparent areas suitable for analysis by electron diffraction. The presence of distinct reflections in the nano-beam diffraction pattern (Figure 2b) and in the selected area diffraction pattern in Figure 2c demonstrates that some regions of the coating have a crystalline character. The obtained diffraction patterns were indexed in terms of the orthorhombic β-$LiAlO_2$ phase (space group *Pna21* (33), $a = 5.28$Å; $b = 6.30$Å; $c = 4.90$Å, PDF file 00-033-0785). The observed HRTEM images provide additional evidence for the existence of crystalline regions in the $LiAlO_2$ coating. A high resolution electron micrograph (HRTEM) of such a crystalline region of the $LiAlO_2$ layer is represented in Figure 3a. An enlarged view of the small area in Figure 3a outlined by a white square is shown in Figure 3b. This image clearly demonstrates the presence of lattice fringes which can be associated with the (211) and (112) planes of the orthorhombic β-$LiAlO_2$ structure identified above on the basis of electron diffraction patterns (Figures 2b, 2c). The "reflection spots" appearing in the Fourier Transform of this area (see insert in Fig. 2a) also unambiguously indicate that the observed region of the coating is crystalline. It should be emphasized that, despite the existence of some crystalline areas, the $LiAlO_2$ coating, as a whole, is amorphous. In Figure 4a, we present grazing incidence angle X-ray diffraction patterns of the $LiAlO_2$ film (~30 nm thick as estimated from STEM image, Figure 1a) on Ni-foil and of bare Ni-foil. One can see that the as-deposited $LiAlO_2$ thin film shows a broad peak between 18° to 25° which is a characteristic peak of an amorphous structure. This is in agreement with the previous results obtained by one of us (V.M.) for as-deposited $Li_xAl_yO_z$ ALD films.[49] It was previously found that the $LiAlO_2$ films are XRD-amorphous when deposited as thin films but they adopt polycrystalline β-$LiAlO_2$ phase when deposited 200-nm or thicker. According to the present study, this crystallization process initiates already in very thin films yet the crystallite size is in nanoscale. In the early stage of the $LiAlO_2$ ALD, the nanoscale crystallites are too small to yield visible diffraction in conventional XRD, but as the film is deposited thicker the growth of $LiAlO_2$ crystallites allows XRD detection. It has been also shown that Li ions are mobile during the $LiAlO_2$ ALD process affecting the material composition and promoting the crystallization and crystallite orientation.[49] Moreover, the absence of any Bragg peak in the 2θ-θ diffraction pattern in Figure 4b, excluding Ni (111) peak, indicates that the film has no preferred growth orientation and is, as a whole amorphous. The 2θ-θ diffraction pattern in the inset of Figure 4b shows three peaks at $2\theta = 44.46°$, $2\theta = 51.81°$ and $2\theta = 76.35°$ which are attributed, respectively to the (111), (200) and (220) reflections of the Ni foil (PDF # 01-010-6148).

Analysis of the electrochemical performance of $LiNi_{0.8}Co_{0.15}Al_{0.05}O_2$ bare and coated $LiAlO_2$/$LiNi_{0.8}Co_{0.15}Al_{0.05}O_2$ electrodes.—Figure 5 presents the results of discharge capacity and Coulombic efficiency measured from $LiNi_{0.8}Co_{0.15}Al_{0.05}O_2$ bare and $LiAlO_2$-coated electrodes cycled at a C/5 rate (30°C) in the potential ranges from 2.7 V to 4.3 V and subsequently to 4.4 V, 4.5 V, with the last 10 cycles once more to 4.3 V, as indicated. Initial 5 formation cycles were carried out at C/15, C/10, and C/5 rates and the voltage profiles of the 1-st cycles to 4.3 V for NCA-bare and NCA/LAO-2 electrodes are demonstrated in Figures 6a and 6b. It is noticeable that in the 1-st cycle (C/15), coated electrodes exhibit lower irreversible capacity loss (ICL) compared to the uncoated ones (11.7 and 14.8%, respectively). In cycling from 2.7 to 4.2 V the latter electrodes display ICL = 12.2% and reversible capacities of

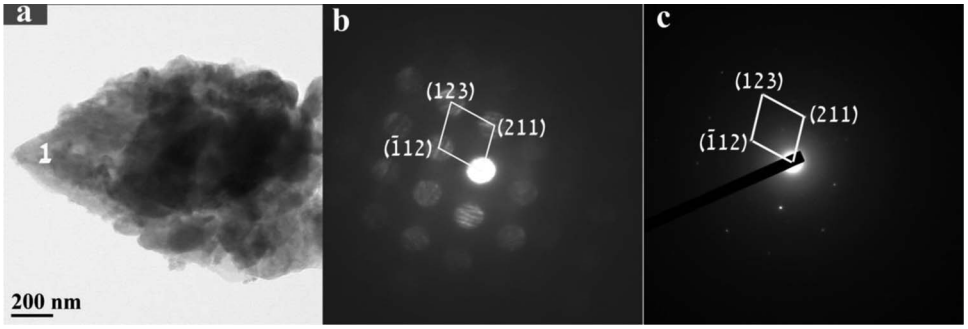

Figure 2. (a) TEM Bright Field image of some agglomerated $LiAlO_2$ particles of the $LiAlO_2$ layer (~30 nm thick) obtained by ALD on the Ni-foil model electrode. (b) Convergent Beam Electron Diffraction (CBED) patterns taken from a ~7 nm area marked **1** in (a) displays reflections that could be assigned to the orthorhombic β-$LiAlO_2$. (c) Selected area diffraction pattern demonstrating that some regions of the coating have a crystalline character.

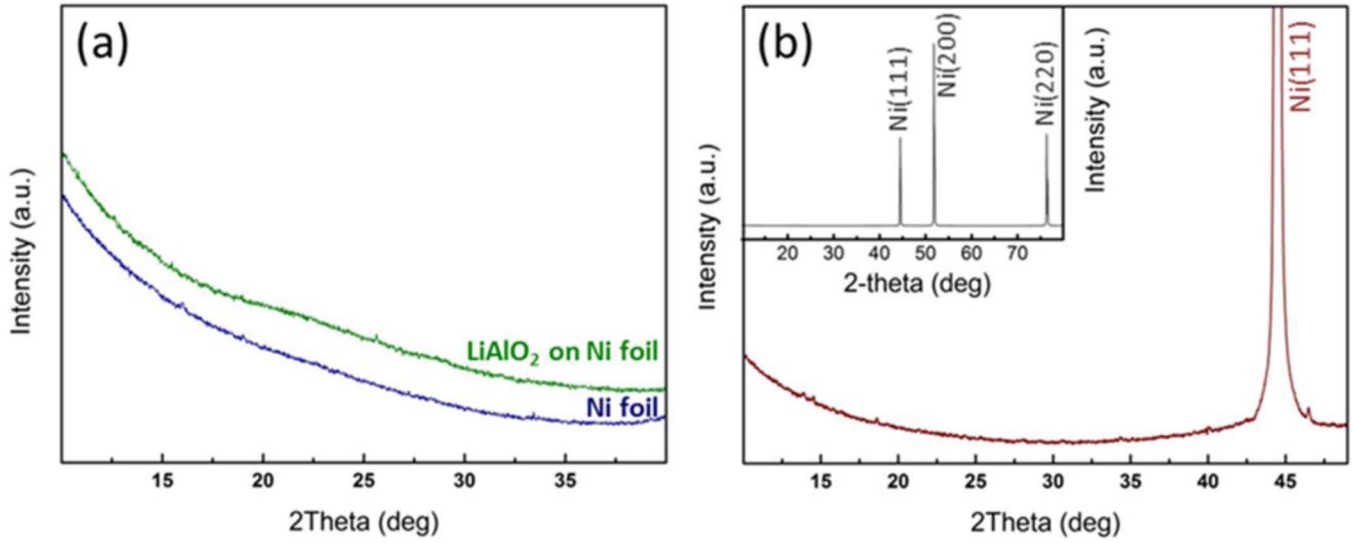

Figure 4. (a) 2-theta scan of the as-deposited $LiAlO_2$ ~30 nm thick film (green) onto Ni foil and of Ni foil (blue), with a grazing-incidence angle of 1.5°, (b) 2-theta-theta scan of the as-deposited $LiAlO_2$ ~30 nm thick film onto Ni foil. *Insert:* The 2θ-θ diffraction pattern exhibiting peaks at $2\theta = 44.46°$, $2\theta = 51.81°$ and $2\theta = 76.35°$ which are attributed, respectively to the (111), (200) and (220) reflections of the Ni foil (PDF # 01-010-6148).

~175 mAh/g at a C/5 rate, established in our preliminary experiments. As it follows from the results of Figure 5, bare and $LiAlO_2$ coated electrodes reveal comparable discharge capacities around 185–190 mAh/g with efficiency of ~99.5% when cycled up to 4.3 V or 4.4 V. Increasing the cutoff voltage to 4.4 V and 4.5 V results, as expected, in increasing the discharge capacity by 10–20 mAh/g, specifically for NCA/LAO-05 and NCA/LAO-1 electrodes (Figure 5). It is important to note that coated electrodes exhibit more stable cycling behavior compared to bare ones when charged to higher potentials (>4.3 V). The most remarkable results in terms of stable capacity and higher Coulombic efficiency of ~99.7% are demonstrated by $LiAlO_2$ coated electrodes with 1 nm and 2 nm thick coatings during cycling in a wide potential window of 2.7–4.5 V (Figure 5). These electrodes exhibit similar voltage profiles measured at 25-th cycle to 4.5 V, slightly higher capacity and increased efficiency of ~99.7% vs. 98% of uncoated electrodes, as shown in Figures 6c and 6d. The results obtained suggest reduced side reactions of the coated NCA/LAO-1 and NCA/LAO-2 electrodes with solution species even at high anodic potentials, when highly oxidized Ni^{4+} ions are formed

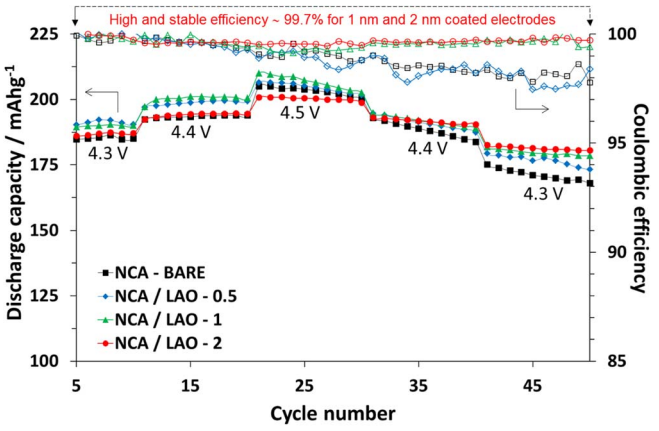

Figure 5. Discharge capacity and Coulombic efficiency measured from NCA bare and ALD coated electrodes NCA/LAO-05, NCA/LAO-1 and NCA/LAO-2 cycled in pouch-type cells at 30°C, C/5 rate, between 2.7 V and 4.3 V and subsequently to 4.4 V, 4.5 V, and yet again to 4.3 V, as indicated. Initial 5 conditioning (formation) cycles from 2.7 to 4.3 V were carried out at C/15, C/10, and C/5 rates.

at the interface as a result of oxidation reactions concomitant with the Li^+ extraction from NCA and other Ni-rich materials.[50] Possible Ni oxidation reactions in the course of charge are indicated in Figure 6c, as follows: Ni^{2+} oxidizes to Ni^{3+} at ~3.6 V and further to Ni^{4+} states at potentials around 3.8–4 V, respectively corresponding to the Li^+ deintercalation levels of x = 0.16–0.32 and x = 0.50 in $Li_{1-x}Ni_{0.8}Co_{0.15}Al_{0.05}O_2$. The bulk-averaged Ni valence at these stages of charge was estimated as +3.1 and +3.7 according to XANES studies by Tonaka et al.[40] At higher potentials of 4.2–4.5 V (x = 0.75–0.80) nickel further oxidizes $Ni^{3+} \rightarrow Ni^{4+}$, thus at the end of charge nickel is at a 4+ state. With respect to cobalt, it was shown from XAS results that the major charge compensation is achieved by the Ni oxidation during Li^+ extraction from $Li_{1-x}Ni_{0.8}Co_{0.15}Al_{0.05}O_2$, while the cobalt ions remain mostly unchanged in the Co^{3+} state even at potentials >4.5 V.[51]

By comparing the differential capacity plots dQ/dV vs. potential of NCA-bare and coated NCA/LAO-2 electrodes for 2-nd and 50-th cycles by charging to 4.3 V (Figure 7), we conclude that similar transition metals oxidation/reduction peaks are developed for these electrodes in deintercalation/intercalation processes. It is important to note that $LiAlO_2$ coated electrodes demonstrate lower capacity fading upon cycling. In addition, we note quite symmetric anodic/cathodic waves at ~3.72–3.74 V of the $Ni^{2+} \leftrightarrow Ni^{3+}$ reactions of these bare and coated samples with comparable potential differences suggesting thus similar electrode kinetics. By close examination of the differential capacity plots we note that the relative integrated area or anodic waves intensity $(dQ/dV)_2/(dQ/dV)_{50}$ of the 2-nd and 50-th cycles at the above potentials (x = 0.3 in $Li_{1-x}Ni_{0.8}Co_{0.15}Al_{0.05}O_2$) is lower for the coated NCA/LAO-2 electrodes (~1.1 vs. 1.4) that can be related therefore to enhanced contribution of the Ni^{2+} and Ni^{3+}-ions in charge compensation in the course of cycling. This may relate likely to the formation of a solid solution between $LiAlO_2$ and $LiNi_{0.8}Co_{0.15}Al_{0.05}O_2$ and to a modified interface developed on the electrodes that promote Li^+ diffusion into the bulk and oxidation/reduction reactions of the Ni-ions. The above phenomena described in Ref. 52 deserve a special study and are beyond the scope of the present work. We suggest that lower irreversible capacity loss of the 1-st cycle and higher efficiency during cycling of $LiAlO_2$ coated electrodes are related partially to reducing side reactions of these electrodes with solutions species. $LiAlO_2$ coatings can protect the active NCA material from direct interactions with protons and trace HF in solutions, for instance:

$$LiAlO_2 + 4HF\,(sol) \rightarrow AlF_3\,(s) \downarrow + 2H_2O + LiF\,(s) \qquad [1]$$

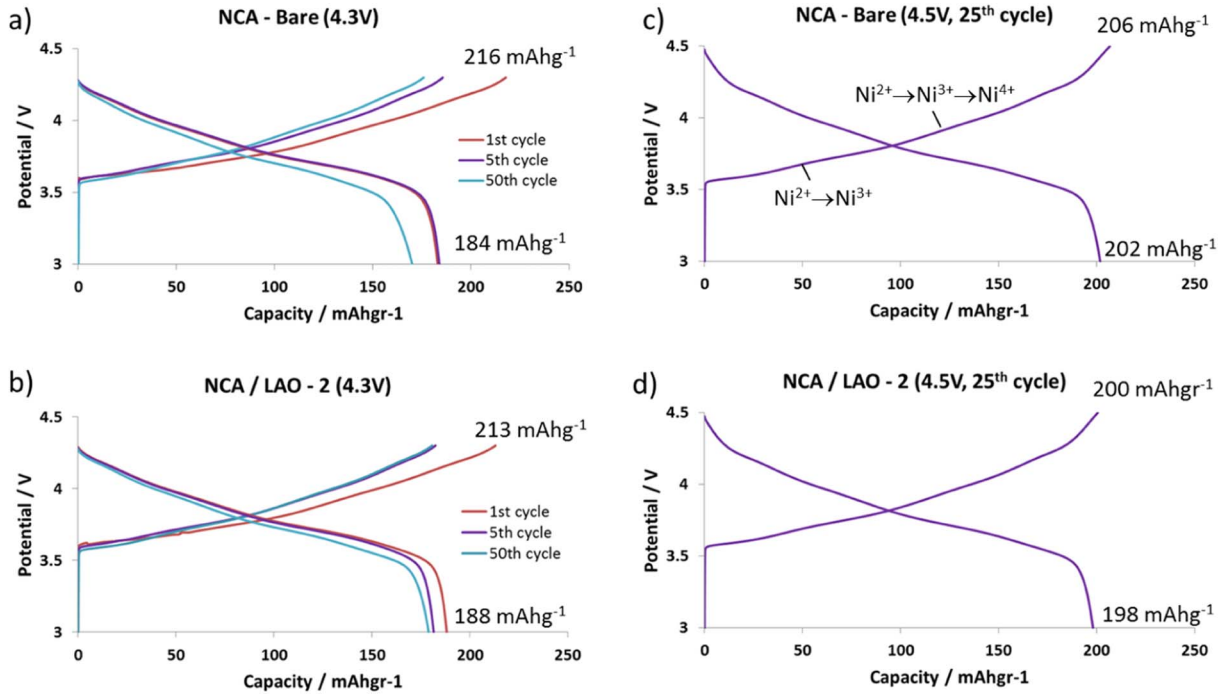

Figure 6. Voltage profiles of several selected cycles measured from NCA bare (a), (c) and ALD coated electrodes NCA/LAO-2 (b), (d) cycled in pouch-type cells at 30°C, C/5 rate, in potential ranges of 2.7–4.3 V and 2.7–4.5 V, as indicated. Possible Ni oxidation reactions upon the Li-ion extraction from NCA at 3.6–4.5 V are shown (Figure 6c) according to Ref. 40.

$$LiAlO_2 + 4H^+ \rightarrow Al^{3+} + Li^+ + 2H_2O \quad [2]$$

$$Al^{3+} + 3HF\,(sol) \leftrightarrow AlF_3\,(s) \downarrow + 3H^+ \quad [3]$$

$$Al^{3+} + Li^+ + 4HF \leftrightarrow LiAlF_4\,(s) \downarrow + 4H^+ \quad [4]$$

Enrichment of a thin reactive surface layer on the coated electrodes with Al^{3+} via Reaction 2 may also initiate the formation of the aluminum fluoride and $LiAlF_4$ species which modifies the electrode/solution interface and results in more stable electrochemical behavior.[10] We have established that 2 nm coated NCA electrodes (NCA/LAO-2) demonstrated ~2–3 times lower capacity fading compared to that of bare and 0.5 nm and 1 nm coated ones, as shown in Figure 8. Our findings are in agreement with the literature data,[53–55] in which the authors demonstrated that coatings increase the voltage window and improve cycling performance of battery materials, like $LiCoO_2$ if powders or composite electrodes were coated with various thin coatings by ALD. These coatings serve as a thin film with low interfacial resistance on the cathode surface, suppress side reactions and electrolyte decomposition mainly at high potentials, prevent the deterioration of cathode structure, resulting therefore in enhanced cyclic stability and low self-discharge.[54] The effectiveness of the $LiAlO_2$ coated NCA-electrodes in terms of more stable cycling and lower capacity fade was confirmed by analysis of impedance measurements represented in Figure 9. We demonstrate impedance spectra of bare and NCA/LAO-2 electrodes measured at several open-circuit potentials during charge (Li^+ deintercalation), up to 4.5 V. Usually, these spectra for practical porous intercalation electrodes consist of two (or sometimes three) semicircles at high (10^5–10^4 Hz) and intermediate

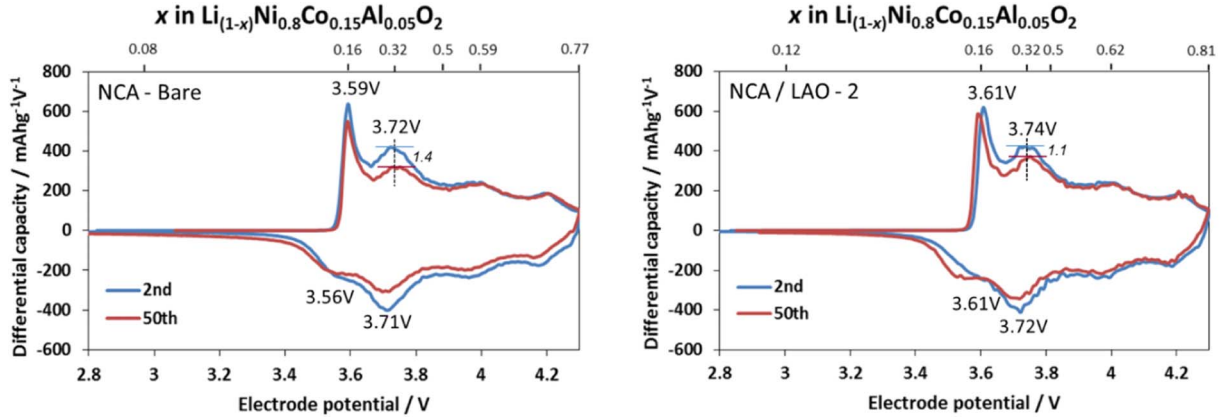

Figure 7. Differential capacity plots of NCA bare and NCA/LAO-2 coated electrodes measured from 2nd and 50th cycles in the potential range of 2.7–4.3 V at 30°C, C/5 rate (see Figure 5). Potentials of characteristic anodic and cathodic waves related to Ni^{2+} oxidation/reduction are indicated. The relative intensities $(dQ/dV)_2/(dQ/dV)_{50}$ of the anodic waves for 2-nd and 50-th cycles at potentials 3.72–3.74 V ($x \approx 0.3$ in $Li_{1-x}Ni_{0.8}Co_{0.15}Al_{0.05}O_2$) of NCA bare and NCA/LAO-2 coated electrodes, calculated as 1.4 and 1.1, respectively, are also indicated.

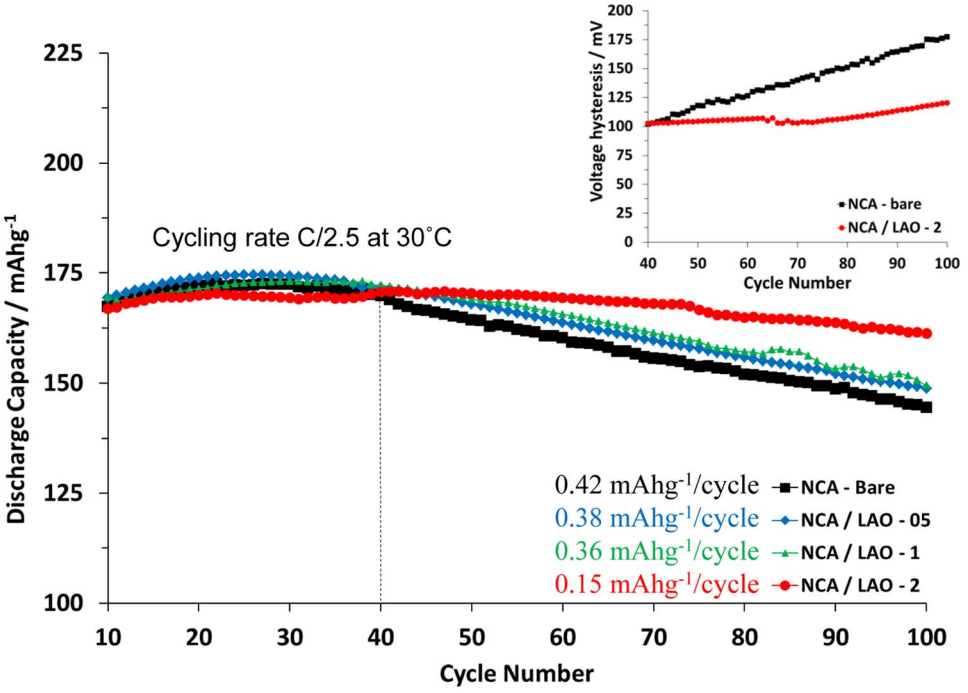

Figure 8. Cycling performance of NCA bare and NCA/LAO-05, NCA/LAO-1 and NCA/LAO-2 coated electrodes at 30°C, C/2.5 rate in the potential range of 2.7–4.3 V. A few formation cycles were performed at C/15 and C/10 rates (see the Experimental section) and are not shown. Capacity fade of the above electrodes calculated for cycle numbers 40^{th}–100^{th} are indicated. For statistical purposes, 3 coin-type cells were used of each type of electrodes and the average values are demonstrated. **Insert:** Comparison of the difference between the mean voltage in charge and mean voltage in discharge (hysteresis) measured for NCA bare and NCA/LAO-2 coated electrodes during cycling at C/2.5 rate (30°C).

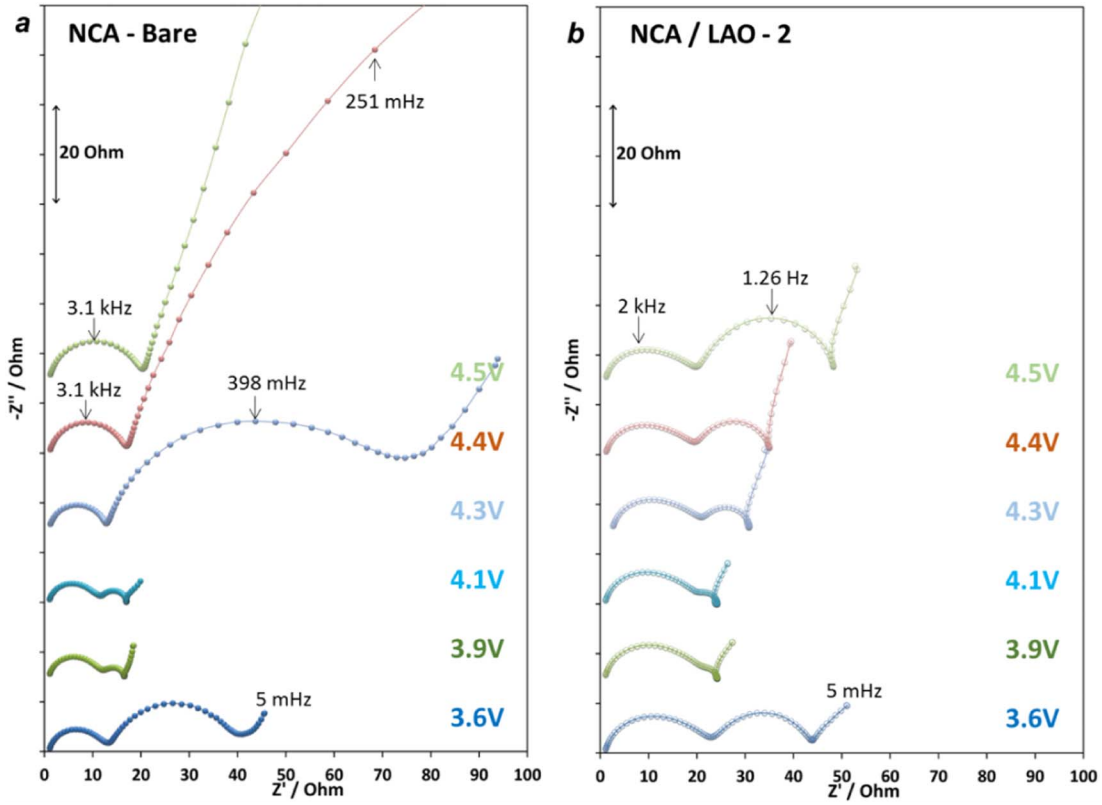

Figure 9. Families of impedance spectra measured at several potentials up to 4.5 V (as indicated) during charge (Li^+ extraction) after 10 cycles (C/5 rate, 30°C) from NCA bare (a) and NCA/LAO-2 coated (b) electrodes. Three-electrode coin-type cells comprising working and counter (Li foil) and reference (Li-chip) electrodes were used, as described in the Experimental section. Selected frequencies of the impedance tests from 100 kHz to 5 mHz are shown. Note much higher total impedance at potentials >4.2 V of NCA bare electrodes comparing to that of 2 nm $LiAlO_2$ coated samples.

(10^3–10^2 Hz) frequencies, respectively and a slope line at very low frequencies (a few mHz range); the latter is attributed to the Li^+ solid state diffusion (Warburg element).[56–58] Figures 10a and 10b compares the resistance that can be related to the interparticle contact of the electrode and to the Li^+ migration through the electrode surface film (R_{sf}, 1-st semicircle), and the resistance of the interfacial reaction (charge-transfer, R_{ct}, 2-nd semicircle) calculated by fitting the above impedance data of bare and coated electrodes. These resistances can be expressed as follows: $R_{sf} = \rho/l \cdot S$ and $R_{ct} = RT/n_e \cdot F \cdot i_0$, where ρ is the resistivity, l–the thickness of the surface film, S–the electrode geometric area, R–the gas constant, T–the temperature, n_e–the number of electron exchange in the processes of lithium ion insertion and extraction, F–the Faraday constant, i_0–the exchange current. It is evident that although R_{sf} of bare electrodes is somewhat lower comparing to that of the coated samples and R_{ct} values are quite comparable for these two types of electrodes in the potential range of 3.6–4.2 V (x≈0.16–0.7 in $Li_{1-x}Ni_{0.8}Co_{0.15}Al_{0.05}O_2$), both these impedance parameters exhibit a remarkable increase for bare electrodes at potentials >4.3 V. We attribute the rise of the charge-transfer resistance for bare NCA electrodes at high potentials to degradation of the electrode/solution interface at high level of the Li^+ extraction, ~80% assuming similar morphological and structural changes of bare and coated NCA electrodes (for instance, formation of a spinel-like phase domains during cycling as demonstrated in the literature[59,60]). In contrast to bare electrodes, R_{ct} measured for the NCA/LAO-2 coated ones remains almost invariant with the electrode potential implying thus structural stability of the interface and lowering activation energy for the charge-transfer of the coated electrodes even at high potentials. These facts correlate well with the improved steady behavior of the 2 nm $LiAlO_2$ coated electrodes cycled to higher potentials of 4.4 and 4.5 V when the delithiation level exceeds 75–80% (Figure 5) and with their stable cycling performance and much lower capacity fading. In contrast, bare NCA electrodes demonstrate more than 2 times higher capacity fade as shown in Figure 8, due to an increased charge-transfer resistance. Our results are in agreement with the data on NCM333 electrodes coated with the Al-oxide.[52] The insert in Figure 8 also demonstrates the remarkably improved electrochemical behavior of the 2 nm $LiAlO_2$ coated electrodes in terms of the lower difference between the mean voltage in charge and mean voltage in discharge (hysteresis) comparing to the uncoated samples upon cycling.

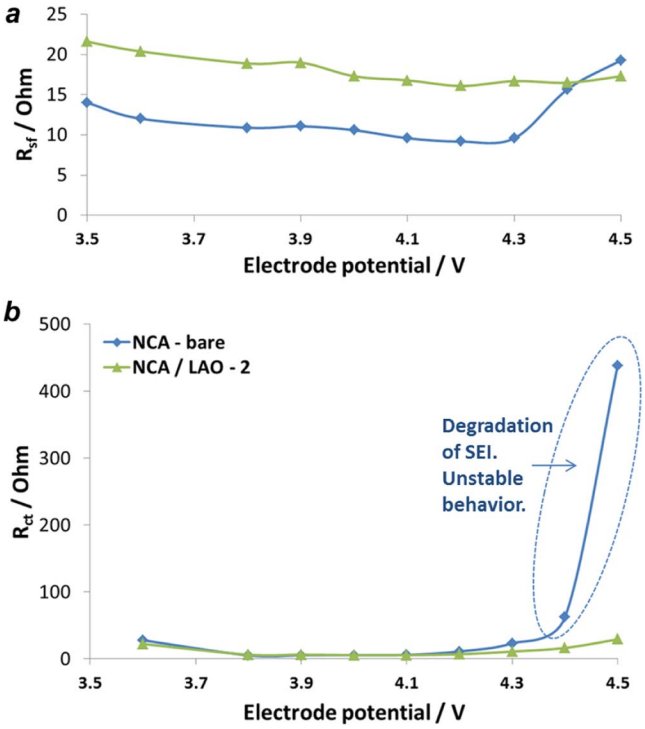

Figure 10. (a) Surface film resistance (R_{sf}) and (b) interfacial charge-transfer resistance (R_{ct}) calculated from impedance spectra of NCA bare and NCA/LAO-2 coated electrodes in Figure 10, as a function of the electrode potential during charge up to 4.5 V. Fitting of the experimental data was performed using ZView software. The electrode potential domain of possible SEI degradation and unstable electrochemical behavior of bare NCA electrodes is indicated with the dash line oval.

We have established that 2 nm-coated NCA electrodes as well as 1 nm-coated samples demonstrated also enhanced performance upon the self-discharge tests for 1 week aging in Li-cells, at 4.3 V under controlled temperatures of 30 and 60°C, after galvanostatic cycling at 30°C. The results are summarized in Figure 11 and in Table I. It

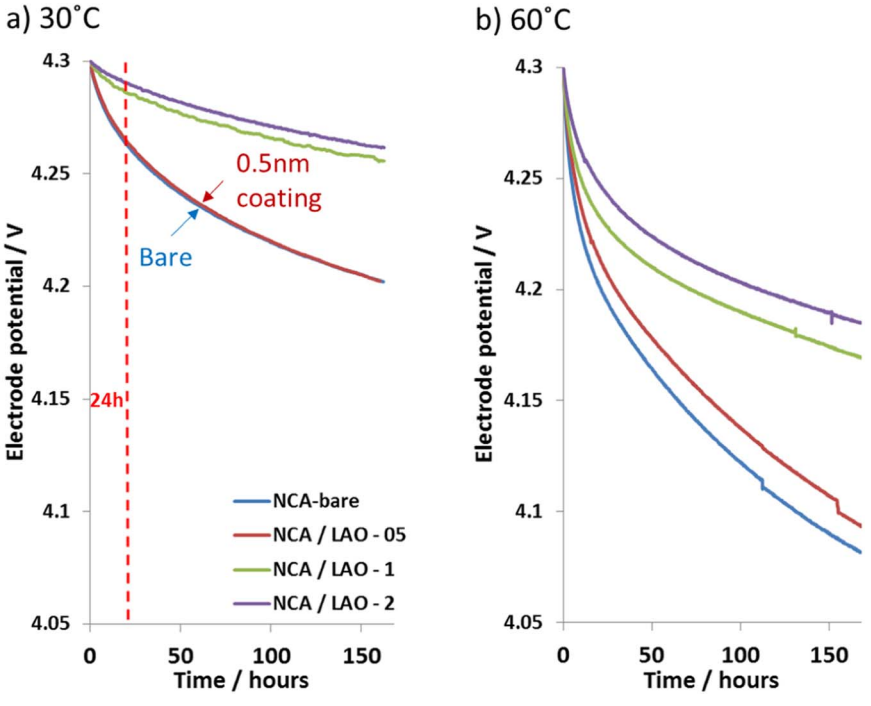

Figure 11. Results of the self-discharge measurements (voltage decay) of NCA bare and NCA/LAO-05, NCA/LAO-1 and NCA/LAO-2 coated electrodes during 1 week at 30°C (a) and 60°C (b), respectively. Detailed comparable characteristics of the self-discharge of these electrodes are shown in Table I.

Table I. Results of the self-discharge/aging during one week of bare NCA and NCA/ALO coated electrodes in coin-type cells at 30 and 60°C.

Sample	Discharge capacity at C/5 before self-discharge, $mAhg^{-1}$	Voltage after 24 h aging, V	Voltage drop after 24 h aging, mV/h	Voltage after one weekaging, V	Voltage drop after one weekaging, mV/h	Average discharge capacity at C/5 after one weekaging, $mAhg^{-1}$	Capacity retention after one weekaging, $mAhg^{-1}$
			7 days at 30°C				
NCA -bare	168.0	4.259	1.71	4.202	0.58	152	90.5%
NCA/LAO –05	173.0	4.269	1.29	4.202	0.58	164	94.7%
NCA/LAO –1	178.5	4.285	0.62	4.255	0.27	167	93.6%
NCA/LAO –2	180.5	4.289	0.46	4.260	0.24	177	98.1%
			7 days at 60°C				
NCA -bare	166.0	4.195	4.38	4.082	1.30	154	92.8%
NCA/LAO –05	175.0	4.208	3.83	4.093	1.23	165	94.3%
NCA/LAO –1	172.0	4.228	3.00	4.169	0.78	160	93.0%
NCA/LAO –2	185.0	4.243	2.38	4.185	0.68	174	94.1%

can be concluded that coated NCA/LAO-1 and NCA/LAO-2 demonstrated much lower values of the electrode potential drop over aging time (dV/dt, mV/h) both for the first 24 hours of the self-discharge and for the 1 week tests. We suggest this is due to decreasing the decomposition reactions of the solution species on the charged electrode coated with $LiAlO_2$ film (2 nm thick). An interesting finding is that there is a correlation between the above parameter (dV/dt) and the thickness of the $LiAlO_2$ film. Namely, electrodes with the thicker film (2 nm) exhibited the lowest voltage drop upon aging electrochemical cells for the first 24 h and subsequently for 7 days, both at 30 and 60°C assuming thus their enhanced stability in reactions with solution species. Additionally, the capacity retention of 2 nm-coated electrodes cycled at 30°C after the self-discharge is also remarkably higher (98.1%) comparing to the bare ones (90.5%). We attribute this to more stable electrode/solution interface developed on the $LiAlO_2$ coated electrodes during cycling/aging and, as a result, to lesser side reactions of these electrodes that correlate well with their improved cycling performance. Our results are in line with those obtained recently for $LiNi_{0.8}Co_{0.1}Mn_{0.1}O_2$ cathode material coated with $LiAlO_2$ that demonstrated its improved electrochemical performance at 40°C.[61]

Analysis by X-ray diffraction of structural changes of $LiNi_{0.8}Co_{0.15}Al_{0.05}O_2$ bare and coated $LiAlO_2$/$LiNi_{0.8}Co_{0.15}Al_{0.05}O_2$ electrodes.—Structural XRD analysis of $LiAlO_2$ coated cycled NCA-samples, as compared to the materials without coating, shows that the main changes caused by cycling are largely described by insignificant deviations in the unit cell parameters (see Table II). A comparison of XRD patterns recorded before and after cycling of uncoated and coated NCA/LAO-2 materials (black/blue profiles and red/green profiles, respectively) is represented in Figure 12. As expected, the observed diffraction patterns can be readily indexed to the rhombohedral $Li(Ni,Co)O_2$ phase with a layered structure described by the *R-3m* space group.[62] Since no essential difference between the profiles is observed, it can be concluded that the structure of uncoated and coated samples, as compared to pristine material, is not changed during cycling, thus meaning that the original structure described by *R-3m* space group is maintained. Moreover, clear splitting of (006)/(102) peaks indicates that the layered structure of the material is preserved at least after 50 charge/discharge cycles.

Table II. Cell parameters calculated from XRD measurements of bare and $LiAlO_2$ coated $LiNi_{0.8}Co_{0.15}Al_{0.05}O_2$ cathodes before (pristine) and after 50 cycles at a C/5 rate (30°C). The parameters were determined by a standard least square refinement procedure.

Electrodes	Parameters of Li (Ni, Co)O_2 phase (hexagonal setting)	
	a(Å)	*c*(Å)
NCA-bare pristine	2.8610	14.1809
NCA-bare after 50 cycles	2.8621	14.1621
NCA/LAO -2 pristine	2.8604	14.1706
NCA/LAO-2 after 50 cycles	2.8610	14.1727

Conclusions

We have demonstrated in this work that $LiAlO_2$ coatings (0.5, 1 and 2 nm thick) were effectively deposited onto practical $LiNi_{0.8}Co_{0.15}Al_{0.05}O_2$ electrodes using ALD method. We have established more stable cycling performance demonstrating efficiency of 99.7% of coated electrodes, especially of NCA/LAO-1 and NCA/LAO-2 during cycling to 4.3–4.5 V. An important conclusion is that upon cycling, 2 nm $LiAlO_2$ coated NCA electrodes displayed ~3 times lower capacity fading and lower voltage hysteresis compared to bare electrodes. On the basis of the main research findings of the comparable electrochemical behavior of bare and coated NCA electrodes we can also conclude that:

1. Lower irreversible capacity loss in the 1-st cycle of 2 nm coated electrodes is related partially to lowering side reactions of these electrodes with solutions species.
2. Much lower interfacial resistance of 2 nm coated electrodes compared to that of bare ones at potentials >4.3 V can be ascribed to enhanced structural stability of the interface and low activation energy for the charge-transfer even at high levels of the Li^+ deintercalation.
3. From the self-discharge studies of these electrodes in charged state at 60°C we concluded on much lower values of the electrode potential drop during aging and on remarkably higher the capacity retention of 2 nm $LiAlO_2$ coated electrodes comparing to the bare ones.
4. Overall, we established a correlation among the thickness of the $LiAlO_2$ film and parameters of the self-discharge processes at 30 and 60°C, namely: the thicker the film is the lower potential drop during aging and the higher the discharge capacity retention values were measured. To the best of our knowledge, these significant research findings were obtained and analyzed for the first time.
5. More stable electrode/solution interface developed on the $LiAlO_2$ coated electrodes during intercalation/deintercalation and aging in a charge state correlates well with their improved cycling performance.
6. Analysis of XRD patterns of bare and coated NCA/LAO-2 electrodes after cycling (C/5 rate, 30°C) allows us to conclude on no structural changes of cycled samples, as compared to pristine materials. Cycled electrodes preserved their original structure described by R-3m space group and no additional phases were detected.
7. Our further research on NCA bare and $LiAlO_2$ coated electrodes will be focused on studies of metal dissolution and structural and

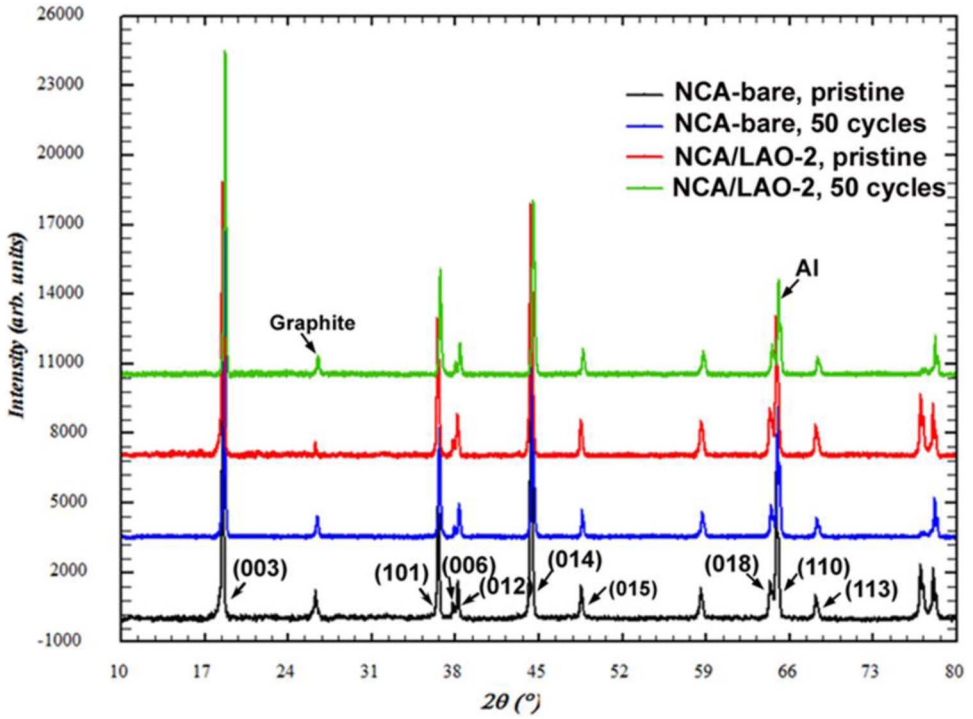

Figure 12. A comparison of XRD profiles (after background subtraction) recorded before and after cycling NCA materials, uncoated and coated with $LiAlO_2$ (2 nm thick coating). Blue and green profiles are referred, respectively, to cycled uncoated and coated electrodes. Black and red patterns are related to NCA bare and NCA/LAO-2 coated pristine electrodes. Peak at $2\theta = 26.5^\circ$ arises from remnants of graphite (4 wt%) in composite NCA electrodes, as noted in the Experimental section.

chemical stability of the $LiAlO_2$ coatings during cycling/aging at elevated temperatures in full cells with graphite negative electrodes.

Acknowledgments

Finnish Centre of Excellence in Atomic Layer Deposition (Academy of Finland) is acknowledged for funding. O.S-L. and B.M. thank Dr. H. Yamin for his interest in this work.

ORCID

Ville Miikkulainen https://orcid.org/0000-0002-9398-2319

References

1. S.-T. Myung, F. Maglia, K.-J. Park, C. S. Yoon, P. Lamp, S.-J. Kim, and Y.-K. Sun, *ACS Energy Lett*, **2**, 196 (2016).
2. V. Etacheri, R. Marom, R. Elazari, G. Salitra, and D. Aurbach, *Energy Environ. Sci.*, **4**, 3243 (2011).
3. A. Manthiram, J. C. Knight, S.-T. Myung, S. Min Oh, and Y.-K. Sun, *Adv. Energy Mater.*, **6**, 1501010 (2016).
4. Z. Liu, A. Yu, and J. Y. Lee, *J. Power Sources*, **81–82**, 416 (1999).
5. N. Yabuuchi and T. Ohzuku, *J. Power Sources*, **119–121**, 171 (2003).
6. T. Ohzuku and Y. Makimura, *Chemistry Letters*, **30**, 642 (2001).
7. N. Yabuuchi, Y. Makimura, and T. Ohzuku, *J. Electrochem. Soc.*, **154**, A314 (2007).
8. L. Wang, Y. Ma, P. Wang, S. Lou, X. Cheng, P. Zuo, C. Du, Y. Gao, and G. Yin, *J. Electrochem. Soc.*, **164**, A1924 (2017).
9. O. Haik, N. Leifer, Z. Samuk-Fromovich, E. Zinigrad, B. Markovsky, L. Larush, Y. Goffer, G. Goobes, and D. Aurbach, *J. Electrochem. Soc.*, **157**, A1099 (2010).
10. D. Aurbach, O. Srur-Lavi, C. Ghanty, M. Dixit, O. Haik, M. Talianker, Y. Grinblat, N. Leifer, R. Lavi, D. T. Major, G. Goobes, E. Zinigrad, E. M. Erickson, M. Kosa, B. Markovsky, J. Lampert, A. Volkov, J.-Y. Shin, and A. Garsuch, *J. Electrochem. Soc.*, **162**, A1014 (2015).
11. D. Wang, X. Li, Z. Wang, H. Guo, Y. Xu, and Y. Fan, *Electrochimica Acta*, **196**, 101 (2016).
12. Y. Zhang and C. Y. Wang, *J. Electrochem. Soc.*, **156**, A527 (2009).
13. S.-H. Lee, C. S. Yoon, K. Amine, and Y.-K. Sun, *Journal of Power Sources*, **234**, 201 (2013).
14. K. Kleiner, J. Melke, M. Merz, P. Jakes, P. Nagel, S. Schuppler, V. Liebau, and H. Ehrenberg, *Appl. Mater. Interfaces*, **7**, 19589 (2015).
15. D. P. Abraham, R. D. Twesten, M. Balasubramanian, L. Petrov, J. McBreen, and K. Amine, *Electrochem. Communications*, **4**, 620 (2002).
16. R. Robert, C. Bünzli, E. J. Berg, and P. Novák, *Chem. Mater.*, **27**, 526 (2015).
17. R. Robert and P. Novak, *J. Electrochem. Soc.*, **162**, A1823 (2015).
18. C. M. Julien, A. Mauger, H. Groult, and K. Zaghib, *Thin Solid Films*, **572**, 200 (2014).
19. Y. Cho and J. Cho, *Journal of The Electrochemical Society*, **157**(6), A625 (2010).
20. Y. Seino, T. Ota, and K. Takada, *Journal of Power Sources*, **196**, 6488, (2011).
21. Z. Chen, Y. Qin, K. Amine, and Y.-K. Sun, *J. Materials Chem*, **20**, 7606 (2010).
22. B. C. Park, H. B. Kim, S. T. Myung, K. Amine, I. Belharouak, S. M. Lee, and Y. K. Sun, *J. Power Sources*, **178**, 826 (2008).
23. S. T. Myung, K. Izumi, S. Komaba, Y. K. Sun, H. Yashiro, and N. Kumagai, *Chemistry of Materials*, **17**, 3695 (2005).
24. Y. Chen, Y. Zhang, B. Chen, Z. Wang, and C. Lu, *J. Power Sources*, **256**, 20 (2014).
25. W. Cho, S. M. Kim, J. H. Song, T. Yim, S. G. Woo, K. W. Lee, J. S. Kim, and Y. J. Kim, *J. Power Sources*, **282**, 45 (2015).
26. J. Xie, A. D. Sendek, E. D. Cubuk, X. Zhang, Z. Lu, Y. Gong, T. Wu, F. Shi, W. Liu, E. J. Reed, and Y. Cui, *ACS Nano*, **11**, 7019 (2017).
27. S. M. George, *Chem. Rev.*, **110**, 111 (2010).
28. X. Li, J. Liu, X. Meng, Y. Tang, M. N. Banis, J. Yang, Y. Hu, R. Li, M. Cai, and X. Sun, *J. Power Sources*, **247**, 57 (2014).
29. L. A. Riley, S. V. Atta, A. S. Cavanagh, Y. Yan, S. M. George, P. Liu, A. C. Dillon, and S.-H. Lee, *Journal of Power Sources*, **196**, 3317 (2011).
30. S. K. Hua, G. H. Chenga, M. Y. Chenga, B. J. Hwanga, and R. Santhanama, *Journal of Power Sources*, **188**, 564 (2009).
31. S. B. Jang, S. H. Kang, K. Amine, Y. C. Bae, and Y. K. Sun, *Electrochimica Acta*, **50**, 4168 (2005).
32. F. Wu, M. Wang, Y. F. Su, L. Y. Bao, and S. Chen, *Electrochimica Acta*, **54**, 6803 (2009).
33. C. Li, H. P. Zhang, L. J. Fu, H. Liu, Y. P. Wu, E. Rahm, R. Holze, and H. Q. Wu, *Electrochim. Acta*, **51**, 3872 (2006).
34. J. S. Park, X. Meng, J. W. Elam, S. Hao, C. Wolverton, C. Kim, and J. Cabana, *Chem. Mater.*, **26**, 3128 (2014).
35. K. Leung, Y. Qi, K. R. Zavadil, Y. S. Jung, A. C. Dillon, A. S. Cavanagh, S.-H. Lee, and S. M. George, *J. Am. Chem. Soc.*, **133**, 14741 (2011).
36. J. Liu and X. Sun, *Nanotechnology*, **26**, 024001 (2015).
37. M. R. Laskar, D. H. K. Jackson, Y. Guan, S. Xu, S. Fang, M. Dreibelbis, M. K. Mahanthappa, D. Morgan, R. J. Hamers, and T. F. Kuech, *Appl. Mater. Interfaces*, **8**, 10572 (2016).
38. G. Dai, H. Du, S. S. Wang, J. Cao, M. Yu, Y. Chen, Y. Tang, A. Li, and Y. Chen, *RSC Advances*, **6**, 100841 (2016).

39. D. Mohanty, K. Dahlberg, D. M. King, L. A. David, A. S. Sefat, D. L. Wood, C. Daniel, S. Dhar, V. Mahajan, M. Lee, and F. Albano, *Scientific Reports*, **6**, 26532 (2016).
40. T. Tonaka, C. Okuda, Y. Seno, K. Koumoto, and Y. Ukyo, *Ceramics International*, **34**, 859 (2008).
41. H. Kondo, Y. Takeuchi, T. Sasaki, S. Kawauchi, Y. Itou, O. Hiruta, C. Okuda, M. Yonemura, T. Kamiyama, and Y. Ukyo, *Journal of Power Sources*, **174**, 1131 (2007).
42. F. Schipper, M. Dixit, D. Kovacheva, M. Talianker, O. Haik, J. Grinblat, E. M. Erickson, C. Ghanty, D. T. Major, B. Markovsky, and D. Aurbach, *J. Mater. Chem. A*, **4**, 16073 (2016).
43. C. Ghanty, B. Markovsky, E. M. Erickson, M. Talianker, O. Haik, Y. Tal-Yossef, A. Mor, D. Aurbach, J. Lampert, A. Volkov, J.-Y. Shin, A. Garsuch, F. F. Chesneau, and C. Erk, *ChemElectroChem*, **2**, 1479 (2015).
44. N. Leifer, O. Srur-Lavi, I. Matlahov, B. Markovsky, D. Aurbach, and G. Goobes, *Chem. Mater.*, **28**, 7594 (2016).
45. D. J. Comstock and J. W. Elam, *J. Phys. Chem. C*, **117**, 1677 (2013).
46. S. Francis Amalraj, B. Markovsky, D. Sharon, M. Talianker, E. Zinigrad, R. Persky, O. Haik, J. Grinblat, J. Lampert, M. Schulz-Dobrick, A. Garsuch, L. Burlaka, and D. Aurbach, *Electrochimica Acta*, **78**, 32 (2012).
47. L. M. Moshurchak, J. R. Dahn, M. Obrovac, and L. Christensen, 208-th ECS Meeting, Abstract #218, **Los Angeles, California**, October 16–21, 2005.
48. H. Gabrisch, T. Yi, and R. Yazami, *Electrochemical and Solid-State Letters*, **11**, A119 (2008).
49. V. Miikuklainen, O. Nilsen, H. Li, S. W. King, M. Laitinen, T. Sajavaara, and H. Fjellvag, *Journal of Vacuum Science & Technology A: Vacuum, Surfaces, and Films*, **33**, 01A101 (2015).
50. M. Dixit, M. Kosa, O. Srur Lavi, B. Markovsky, D. Aurbach, and D. T. Major, *Phys. Chem. Chem. Phys.*, **18**, 6799 (2016).
51. W.-S. Yoon, K. Y. Chung, J. McBreen, D. A. Fischer, and X.-Q. Yang, *J. Power Sources*, **174**, 1015 (2007).
52. A. Yano, S. Aoyama, M. Shikano, H. Sakaebe, K. Tatsumi, and Z. Ogumi, *J. Electrochem. Soc.*, **162**, A3137 (2015).
53. Scott Isaac David, "Electrochemical Effects of Atomic Layer Deposition on Cathode Materials for Lithium Batteries" (2013). Mechanical Engineering Graduate Theses & Dissertations. 65. http://scholar.colorado.edu/mcen_gradetds/65.
54. X. Li, J. Liu, X. Meng, Y. Tang, and X. Sun, *J. Power Sources*, **247**, 57 (2014).
55. Y. S. Jung, A. S. Cavanagh, L. A. Riley, S.-H. Kang, A. C. Dillon, M. D. Groner, S. M. George, and S.-H. Lee, *Adv. Mater.*, **22**, 2172 (2010).
56. M. D. Levi and D. Aurbach, *J. Phys. Chem. B*, **101**, 4630 (1997).
57. M. D. Levi, G. Salitra, B. Markovsky, H. Teller, D. Aurbach, U. Heider, and L. Heider, *J. Electrochem. Soc.*, **146**, 1279 (1999).
58. F. Amalraj, M. Talianker, B. Markovsky, L. Burlaka, N. Leifer, G. Goobes, E. M. Erickson, O. Haik, J. Grinblat, E. Zinigrad, D. Aurbach, J. K. Lampert, J.-Y. Shin, M. Schulz-Dobrick, and A. Garsuch, *J. Electrochemical Soc.*, **160**(11) A2220 (2013).
59. E. Jo, S. Hwang, S. M. Kim, and W. Chang, *Chem. Mater.*, **29**, 2708 (2017).
60. H. Zhang, K. Karki, Y. Huang, M. S. Whittingham, E. A. Stach, and G. Zhou, *J. Phys. Chem. C*, **121**, 1421 (2017).
61. Z. Xiao, C. Hu, L. Song, L. Li, Z. Cao, H. Zhu, J. Liu, X. Li, and F. Tang, *Ionics*, 2017, DOI 10.1007/s11581-017-2178-7.
62. A. Rougier, I. Saadoune, P. Gravereau, P. Willmann, and C. Delmas, *Solid State Ionics*, **90**, 83 (1996).